Ab initio structure and energetics of Pu(OH)$_4$ and Pu(OH)$_4$(H$_2$O)$_n$ clusters: Comparison between density functional and multi-reference theories

Patrick Huang *, Mavrik Zavarin, Annie B. Kersting

Physical and Life Sciences Directorate, Lawrence Livermore National Laboratory, 7000 East Ave., Livermore, CA 94550, United States

ABSTRACT

The electronic and geometric structure of the Pu(OH)$_4$ molecule and Pu(OH)$_4$(H$_2$O)$_n$ ($n = 1 - 19$) clusters are compared using a range of single- and multi-reference theories. We find that single-reference methods such as unrestricted, second-order Møller–Plesset perturbation theory provide a reasonable description, and explicit inclusion of multi-configurational effects involving Pu 5f-electrons is not essential. However, density functional theory (DFT) with standard approximations for exchange–correlation performs poorly for Pu(OH)$_4$ and Pu(OH)$_4$(H$_2$O)$_n$ clusters. We propose the use of DFT + U as a simple improvement over standard DFT, and determine an *ab initio* parameterization of DFT + U suitable for atomistic simulations of Pu(OH)$_4$ in aqueous environments.

© 2012 Elsevier B.V. All rights reserved.

1. Introduction

The presence of plutonium (Pu) in the environment due to anthropogenic activity remains a serious problem, and efforts to predict the transport and fate of Pu require an understanding of the dominant biogeochemical processes that regulate its behavior [1]. However, the aqueous chemistry of Pu is quite complicated [2,3]. Pu can assume at least four formal oxidation states in water (+3, +4, +5, +6), each with its own distinct characteristics. In groundwater, Pu concentrations have been observed in the range of $\sim 10^{-12} - 10^{-15}$ M [4–6]. Detailed characterization of Pu is difficult at such low concentrations, and experiments are typically conducted at Pu concentrations $\gg 10^{-12}$ M [7]. This is especially problematic for the highly insoluble species Pu(IV); at such concentrations tetravalent actinide ions such as Pu(IV) have a strong tendency towards hydrolysis, polymerization, and colloid formation in solution. Little direct information is available on the nature of Pu(IV) at low environmental concentrations, and the practice of extrapolating laboratory results at high concentrations to the low concentrations found in the field has yet to be validated.

The motivation for this work is the elucidation of the chemical nature and reactivity of aqueous Pu(IV) at environmentally relevant conditions, i.e., down to the femtomolar regime where experimental characterization is difficult. Pu(IV) can exist as both a monomeric species or in colloid form under a range of aqueous environments. At neutral to alkaline pH, which is the relevant pH range for natural waters, the fully hydrolyzed species Pu(OH)$_4$(aq) is expected to be the predominant form at the solubility limit of amorphous Pu(IV) oxide and in the absence of complexing ligands [8]. Under such cir-

cumstances, estimates for the saturation concentration of monomeric Pu(OH)$_4$(aq) are in the range of log[Pu(OH)$_4$(aq)] = $-10.4 \pm$ 0.5, based on selected experimental values for the solubility product of amorphous Pu(IV) hydroxide and aqueous Pu(IV) hydrolysis constants [8]. As Pu(IV) can be found in the field at concentrations below this solubility limit, the monomeric Pu(OH)$_4$(aq) species is expected to play an important role in the aqueous environmental chemistry of Pu(IV), and is therefore the subject of this study.

To this end, *ab initio* simulations are a promising tool for the study of aqueous actinide ions [9,10]. However, the electronic structure of actinide complexes poses significant challenges. High-Z elements exhibit large relativistic and spin–orbit coupling effects, and the description of open-shell f-electrons is difficult due to strong correlation effects. Accurate treatment of actinide complexes requires sophisticated correlated wavefunction techniques whose computational cost grows rapidly with the number of electrons, and are only practical for isolated, small complexes. To date, much of the theoretical work has examined on the actinyl complexes AnO$_2^+$ and AnO$_2^{2+}$ and their analogs, for which gas phase experiments are available for direct comparison [11]. Theoretical studies of the insoluble Pu(IV) species have focused on complexes at low pH, e.g., aquo complexes [12,13], which can be produced at sufficiently high concentrations for experimental characterization [14–16].

Ultimately, we are interested in simulating the atomic-scale behavior of aqueous Pu in condensed phases. The aqueous solvation of metal ions is typically modeled using cluster approaches, which involve the explicit treatment of the ion and one or more hydration shells, possibly embedded in a continuum dielectric representation for the solvent environment. Cluster models have been extensively applied to the study of aqueous actinide ions (e.g., Ref. [10] and references therein), and have the advantage that they are

* Corresponding author. Fax: +1 925 423 5733.
E-mail address: huang26@llnl.gov (P. Huang).

amenable to the hierarchy of wavefunction-based quantum chemical methods for the systematic treatment of electron correlation.

More recently, advances in large-scale *ab initio* molecular dynamics techniques have lead to the increasing use of periodic supercell models to study metal ions in aqueous environments, and are easily generalized to interfacial phenomena. One drawback of periodic models is that they are not easily amenable to correlated wavefunction methods, and typically density functional theory (DFT) within the local density approximation (LDA) or generalized gradient approximation (GGA) is employed. While this is usually sufficient for simple alkali [17] and alkali earth cations [18,19] or closed shell actinide complexes such as UO_2^{2+} [20], both LDA and GGA can give large errors when strongly correlated *d*- or *f*-electrons are involved ("self-interaction error"). Hybrid functionals and the more recent range-separated hybrids can improve on the LDA and GGA, but this improvement is neither guaranteed nor systematic. Moreover, the significantly higher computational cost associated with hybrid functionals restricts their present use in large-scale dynamical simulations, although ongoing efforts to overcome this technical limitation appear promising [21–23].

Alternatively, in the solid state, the extension of DFT to explicitly include on-site interactions (DFT + U) has been successful in improving the description of strongly correlated materials at a computational cost comparable to the usual LDA or GGA [24]. We propose the use of DFT + U as a practical means to study actinide ions in *aqueous* conditions, and explore how to parameterize DFT + U for $Pu(OH)_4$(aq). Starting with the $Pu(OH)_4$ molecule as a benchmark case, we compare various correlated wavefunction and DFT-based electronic structure methods and examine whether explicit multi-configurational correlations are necessary, or whether a single-reference theory is sufficient. The influence of varying approximations for electron correlation is then explored in benchmark calculations on small $Pu(OH)_4(H_2O)_n$ clusters. Finally, we describe the development and parameterization of a DFT + U model suitable for the large-scale simulation of $Pu(OH)_4$ in aqueous environments.

2. Methods

The core electrons of Pu are replaced with a scalar relativistic effective core potential (ECP). Most calculations here are carried out using the large-core ECP of Hay and Martin [25], which replaces 78 core electrons, leaving 12 valence electrons for Pu(IV). The Pu 6*s*, 6*p*, and 5*f* electrons are treated as valence using the basis set associated with this ECP. Hay and Martin used a [3*s*3*p*2*d*2*f*] contraction; here, we uncontract the two outermost *s* and *p* primitives to yield a [4*s*4*p*2*d*2*f*] contraction. In a few cases we have also made comparisons with the small-core Stuttgart ECP and basis set, which replaces 60 core electrons [26,27]. Double-zeta correlation consistent basis sets (cc-pVDZ) are used for all electrons of O and H [28]. The O atoms of OH⁻ are augmented with diffuse functions (aug-cc-pVDZ) in order to give a good description of the excess negative charge on the O. Enlarging the basis set to triple-zeta with diffuse functions (aug-cc-pVTZ) on all O and H atoms changes bond distances by about 0.01 Å or less for the $Pu(OH)_4(H_2O)$ cluster; as discussed further below, this is smaller than the effects of varying approximations for electron correlation. All calculations involving the large-core ECP are done using the general atomic and molecular electronic structure system (GAMESS) [29]. The small-core ECP requires the evaluation of integrals involving higher angular momentum components that are not presently implemented in GAMESS, and thus the small-core ECP calculations are carried out using the GAUSSIAN 03 code [30].

The complete active space self-consistent field (CASSCF) method [31,32] explicitly accounts for the multiconfigurational character of the Pu 5*f*-electrons. Several different choices for the active spaces are tested; these are discussed further in Section 3.1 below. The optimized CASSCF wavefunction is used as reference for second-order, multi-reference Møller–Plesset (MRMP) perturbation theory [33], which is suitable for capturing dynamical correlation effects. In the MRMP calculations, the O 1*s* electrons are left uncorrelated, while the remaining electrons are correlated. The MRMP is the highest level of theory we employ here and serves as the benchmark against which more approximate approaches are compared. We also consider unrestricted Hartree–Fock (UHF) starting from the dominant determinant of the optimized CASSCF wavefunction, as well as unrestricted, second-order Møller–Plesset perturbation theory (MP2) using the optimized UHF wavefunction as reference. For the density functional theory (DFT) calculations, two common exchange–correlation functionals are employed here: the generalized gradient approximation (GGA) of Perdew, Burke, and Ernzerhof (PBE) [34] and the hybrid extension of this, PBE0 [35]. The numerical evaluation of atomic integrals are carried out on a Lebedev grid spanning 96 radial points and 302 angular points. Vibrational Hessian analysis is performed on all optimized structures to verify their stability.

As our task is to compare the description of electron correlation across varying levels of theory for the ground electronic state, this is most clearly done without additional complications due to spin–orbit effects, which we neglect here. While the inclusion of spin–orbit effects are essential for a qualitative description of electronic excited states, previous theoretical studies of small actinide complexes generally find that the effects of spin–orbit coupling are to modify geometries in the ground electronic state by <0.1 Å and vibrational frequencies by a few percent [10,36,37].

3. Results and discussion

3.1. Pu(OH)4 molecule

We begin by examining two high-symmetry structures of $Pu(OH)_4$ across different levels of theory: tetrahedral and planar (Figure 1). In general, tetrahedral coordination complexes minimize ligand–ligand repulsion and are favored in the case of bulky ligands or when the metal–ligand bond is primarily ionic in character. The planar form can be obtained by flattening the tetrahedral structure. The geometry of the tetrahedral structure is optimized under T_d symmetry, while the planar structure is optimized under D_{2h} symmetry. Table 1 summarizes the equilibrium bond distances and angles derived from six different levels of theory. In all cases, tetrahedral $Pu(OH)_4$ with Pu–O–H bond angle at 180° is found to be the ground state, with the planar structure higher in energy. Analysis of the vibrational Hessian matrix indicates that the tetrahedral structure is a stable minimum, while the planar structure is a transition state for inversion of the tetrahedral structure.
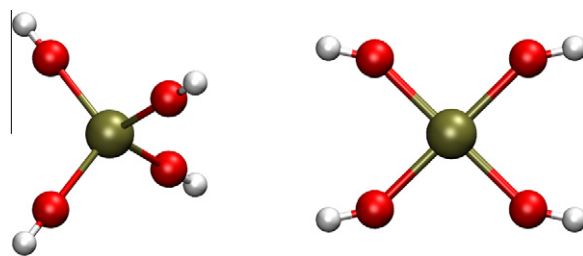

Figure 1. Tetrahedral (left) and planar (right) $Pu(OH)_4$, having T_d and D_{2h} symmetries, respectively. The tetrahedral structure is the ground state, and the planar structure is the transition state for the inversion of tetrahedral structure.

Table 1
Bond distances (in Å) and angles (in deg) for tetrahedral (tet) and planar (pl) Pu(OH)$_4$, and their energy difference (in eV), derived from varying treatments of electron correlation (Section 2). O$_h$ denotes hydroxyl oxygen.

	CAS (4/7)	MRMP	UHF	MP2	PBE	PBE0
Tetrahedral T_d						
Pu–O$_h$	2.10	2.08	2.10	2.08	2.17	2.11
O$_h$-H	0.94	0.96	0.94	0.96	0.97	0.96
Planar D_{2h}						
Pu–O$_h$	2.13	2.11	2.13	2.11	2.20	2.14
O$_h$-H	0.94	0.96	0.94	0.96	0.98	0.96
∠(PuOH)	147.8	145.2	144.0	141.4	123.3	126.5
$E_{pl} - E_{tet}$	1.52	1.32	1.48	1.34	0.52	0.70

CASSCF provides a general way to account for correlations between Pu 5f-electrons; in the case of Pu(IV) this involves four open-shell 5f-electrons. The initial molecular orbitals for the CASSCF wavefunction were taken from a restricted open-shell Hartree–Fock (ROHF) calculation for the high-spin ($S_z = 2$) configuration with the lowest energy. For the tetrahedral structure this is an $(a_1)^1(t_2)^3$ configuration; for the planar structure this corresponds to an $(a_u)^1(b_{1u})^1(b_{2u})^1(b_{3u})^1$ configuration. We begin with a CASSCF wavefunction that includes all possible occupations of four 5f-electrons in seven 5f-orbitals, which we refer to as a CAS (4/7) active space. For the tetrahedral structure, the CASSCF ground state wavefunction is dominated by the initial ROHF configuration but with a reduced weight of $|c_i|^2 = 0.91$. For the planar structure, the ROHF configuration also dominates but with a weight reduced to $|c_i|^2 = 0.81$. Inclusion of dynamical correlations with MRMP produces small (0.02 Å) changes in bond lengths, while decreasing the energy difference between the two structures by 0.2 eV.

While the CAS (4/7) active space allows for correlations between Pu 5f-electrons, correlations involving the oxygen sp-electrons are not explicitly included. To assess their significance, four doubly occupied oxygen orbitals from the ROHF wavefunction were identified by inspection as having the suitable shape and symmetry to form bonding/antibonding combinations with the Pu 5f-orbitals (Figure 2). These orbitals were added the CAS (4/7) active space to form a CAS (12/11) active space. Optimization of the CAS (12/11) wavefunction produced negligible changes to the weights of the dominant configurations and bond lengths (<0.001 Å) as compared to the CAS (4/7) wavefunction, and the natural occupation numbers of the oxygen orbitals that were moved into the active space remained very close to two. Thus, it appears that bonding interactions involving the Pu 5f-orbitals are not significant here, and that the smaller CAS (4/7) active space is sufficient; the Pu-oxygen interaction is likely dominated by electrostatics arising from the large formal charge on Pu(IV).

As the CASSCF wavefunctions are largely dominated by a single electronic configuration, we examine whether a single-reference theory based on the dominant CASSCF configuration can provide a reasonable description of the electronic structure. These results are summarized in Table 1. The main difference between unrestricted Hartree–Fock (UHF) and CAS (4/7) is the neglect of near-degenerate Pu 5f-configurations in the single-determinant UHF; both UHF and CAS (4/7) do not correlate the OH$^-$ electrons. Including correlations via unrestricted MP2 gives excellent agreement with MRMP. While the CASSCF weights for the dominant configurations deviate appreciably from unity, it appears that this is not due to the presence of near-degeneracies, and the good agreement between CAS (4/7) and UHF and between MRMP and MP2 indicates that a single-reference treatment is sufficient for both the tetrahedral and planar structures. The behavior of DFT with standard approximations for exchange–correlation is more problematic, with the largest errors coming from the PBE approximation. The Pu–O$_h$ bond length from PBE is longer by
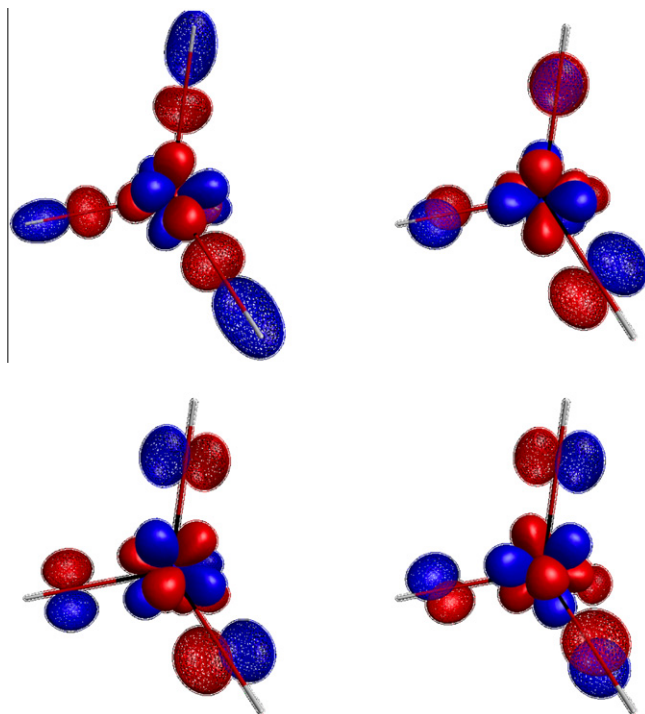

Figure 2. Oxygen sp-orbitals (mesh surfaces) added to the CAS (4/7) active space to form the CAS (12/11) active space. Each oxygen sp-orbital is plotted on the same frame as the corresponding Pu 5f-orbital (solid surfaces) with suitable shape and symmetry for σ-type interaction (upper left) or π-type interactions (upper right, lower left, lower right).

almost 0.1 Å as compared to MRMP. Another issue is the energetics: for PBE the energy barrier between the two structures is underestimated relative to MRMP by more than 50%. The hybrid functional PBE0 gives better agreement with MRMP for geometries, but the barrier is still too low compared to MRMP.

These problems are due to the self-interaction error inherent in approximate exchange–correlation functionals, which can be large when localized states are involved. This is more clearly seen by comparing the highest occupied molecular orbital (HOMO) from the set of optimized MP2 orbitals with the HOMO from PBE (Figure 3). The HOMO from MP2, which is free of self-interaction errors, is largely oxygen sp in character. In contrast, the PBE HOMO possesses much more Pu 5f-character, a typical self-interaction effect [38]. This is due to the tendency of the self-interaction error to destabilize the energies of orbitals with significant localized character, shifting these states toward the HOMO level. The large underestimation of the energy difference $E_{pl} - E_{tet}$ can be attributed
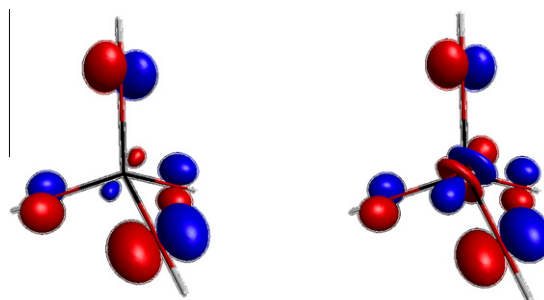

Figure 3. Highest occupied molecular orbital (HOMO) for tetrahedral Pu(OH)$_4$ from the set of optimized MP2 orbitals (left) and PBE (right). The greater localized Pu 5f-character in the PBE is a typical self-interaction effect, which tends to destabilize localized states and shift them towards the HOMO [38].

to the inexact cancellation of self-interaction errors between the planar and tetrahedral $Pu(OH)_4$ structures.

3.2. $Pu(OH)_4(H_2O)_n$ clusters

While unrestricted MP2 theory provides a good description of $Pu(OH)_4$ as shown above, we are ultimately interested in a practical means to study the chemistry of $Pu(OH)_4$ in aqueous environments. As the computational cost of MP2 makes it impractical for large-scale condensed phase simulations, it becomes necessary to explore more approximate strategies. Here, we consider small $Pu(OH)_4(H_2O)_n$ ($n = 1−3$) clusters as model benchmark systems, and restrict the attention to equilibrium geometries, which are generally much less sensitive to basis set incompleteness issues. Results for Pu–oxygen bond distances are summarized in Table 2, where O_h and O_w denote hydroxyl and water oxygens, respectively.

As with $Pu(OH)_4$, the largest discrepancies in the Pu–O_h distances are again due to the PBE approximation, which differ by ~0.1 Å relative to MP2. For $n = 1, 2$, the Pu–O_w distances from PBE0 are in excellent agreement with MP2. The $n = 3$ cluster is more complicated as two distinct, stable structures are found: (1) four hydroxyls and two water molecules in the inner coordination shell (coordination number CN = 6) with the third water in the second shell, and (2) all four hydroxyls and three water molecules in the inner shell (coordination number CN = 7). Both UHF and MP2 predict CN = 7 to be the lowest energy structure, with the CN = 6 structure higher in energy by 0.21 eV for UHF and 0.24 eV for MP2. Inclusion of harmonic zero-point corrections lowers the UHF value slightly to 0.19 eV and changes the MP2 value by less than 0.01 eV. While the UHF errors for the Pu–O_w distances in the $n = 3$ clusters are appreciable, the relative stabilities of the CN = 6, 7 structures from UHF are in good agreement with MP2.

On the other hand, PBE and PBE0 predicts the opposite: the CN = 6 structure is favored by 0.11 eV and 0.06 eV, respectively; harmonic zero-point corrections raise these energy differences slightly to 0.12 eV for PBE and 0.08 eV for PBE0. As such energies are rather small, we investigate this further with a larger basis set: aug-cc-pVDZ on all O and H, plus an additional diffuse f-function with exponent of 0.05 on Pu [13]. The results are very similar: the CN = 6 structure is lower in energy by 0.15 eV and 0.05 eV from PBE and PBE0, respectively. Thus, qualitative discrepancies from the DFT-based methods are already evident for these small benchmark clusters. We also make comparisons with the small-core Stuttgart ECP and basis set, which replaces 60 core electrons of Pu; these results are shown in the last column of Table 2. Bond

distances are in agreement to within ~0.02 Å or less, and thus errors due the large-core approximation are less important compared to the errors due to the PBE and PBE0 approximations.

The above examples demonstrate that standard DFT functionals can lead to qualitatively incorrect predictions for $Pu(OH)_4$-water. Unfortunately, DFT with local or semilocal approximations remain the most practical *ab initio* method of choice for the large-scale simulation of condensed phases. The additional computational expense associated with the evaluation of Fock exchange under periodic boundary conditions limits the applicability of Hartree–Fock or hybrid DFT exchange–correlation functionals, although efforts to overcome this are ongoing [21–23]. In solid-state problems, it has long been known that a simple way to correct for strong on-site correlations is the DFT + U method [24]. This involves the introduction of additional Hubbard-like parameters U and J, which can be interpreted as the screened Coulomb and exchange energies associated with some chosen set of localized states. While there are comparatively fewer applications of DFT + U to molecular problems, the use of DFT + U for transition metal complexes has been reported in more recent years [39,40]. As the computational expense of DFT + U is comparable to standard DFT, this is a potentially useful strategy for the simulation of actinide ions in condensed phases.

A number of different formulations of the DFT + U energy functional has been proposed which largely differ in the way double-counting contributions are subtracted off. Here, we consider the DFT + U formulation of Dudarev et al. [41] within the PBE for exchange–correlation,

$$E_{\text{DFT}+U} = E_{\text{DFT}} + \frac{U-J}{2}\sum_{\sigma}[\text{Tr}(\rho^{\sigma}) - \text{Tr}(\rho^{\sigma}\rho^{\sigma})], \tag{1}$$

where U and J are the spherically-averaged screened Coulomb and exchange energies, respectively, and ρ^{σ} is the density matrix of f-electrons. The difference $U − J$ is regarded as a free parameter that is typically chosen by fitting to some known quantity from experiment. For example, a value of $U − J = 4$ eV has been found to yield reasonable equilibrium ground state properties of solid PuO_2 [42,43]. For the liquid state however, it is less clear how to choose an appropriate parameterization for $U − J$.

As an alternative to fitting to experiments, $U − J$ can also be evaluated from first principles, either via constrained DFT [39,44] or from Hartree–Fock theory [45,46]. The latter has the advantage of being self-interaction-free and is therefore the approach we adopt here. We consider the local influence on $U − J$ due to the presence of nearby water molecules, which is modeled as $Pu(OH)_4(H_2O)_n$ clusters. Following the prescription of Mosey and Carter, U and J are directly evaluated from UHF theory by drawing a correspondence with the UHF Coulomb and exchange integrals, as implemented in a modified version of the GAMESS code [46].

Given that UHF predicts equilibrium structures that are in qualitative agreement with MP2 for small $Pu(OH)_4(H_2O)_n$ ($n = 1−3$) clusters, we employ UHF to carry out the geometry optimization of larger clusters of $n = 7−19$ water molecules, with the largest $n = 19$ cluster shown in Figure 4. This cluster has enough water molecules to complete a second solvation shell and begin filling in a third shell. At this size, the essential features of the inner coordination shell appear converged: there are four hydroxyl and three water molecules in the inner shell, with two of the hydroxyls occupying the axial positions while the other two hydroxyls and three waters are arranged around the equatorial positions, reminiscent of the hydration structure of linear actinyl ions [2].

Figure 5 shows the calculated $U − J$ for $Pu(OH)_4(H_2O)_n$ as a function of the number of water molecules n, which approaches $U − J = 5.4$ eV at the largest $n = 19$ cluster. Inclusion of a polarizable continuum model (PCM) [47] to represent the solvent

Table 2
Mean absolute error (MAE) of Pu–O_h and Pu–O_w bond lengths (in Å) for $Pu(OH)_4(H_2O)_n$ ($n = 1 − 3$) clusters relative to unrestricted MP2. O_h and O_w denote hydroxyl and water oxygens, respectively. For $n = 3$, two structures are found: (1) four hydroxyls and two water molecules in the inner coordination shell (coordination number CN = 6) with the third water in the second shell, and (2) all four hydroxyls and three water molecules in the inner shell (coordination number CN = 7). Values in the last column are MAEs from unrestricted MP2 between the large- and small-core effective core potentials (SC-ECP).

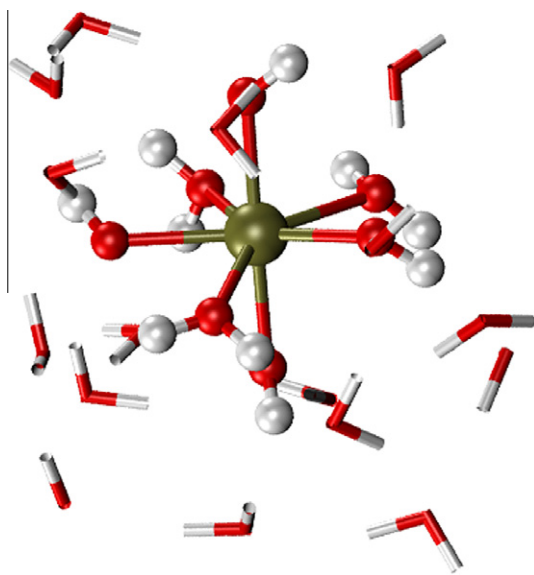|	UHF	PBE	PBE0	MP2 (SC-ECP)
Pu–O_h				
$n = 1$	0.018	0.096	0.026	0.016
$n = 2$	0.016	0.095	0.025	0.010
$n = 3$, CN = 6	0.029	0.078	0.035	
$n = 3$, CN = 7	0.022	0.10	0.030	0.018
Pu–O_w				
$n = 1$	0.024	0.037	0.0060	0.021
$n = 2$	0.036	0.022	0.0046	0.021
$n = 3$, CN = 6	0.096	0.085	0.055	
$n = 3$, CN = 7	0.056	0.060	0.018	0.011

Figure 4. $Pu(OH)_4(H_2O)_{19}$ cluster optimized at the UHF level of theory. Four hydroxyl and three water molecules are found in the inner shell, with two of the hydroxyls occupying the axial positions while the other two hydroxyls and three waters are arranged around the equatorial positions.
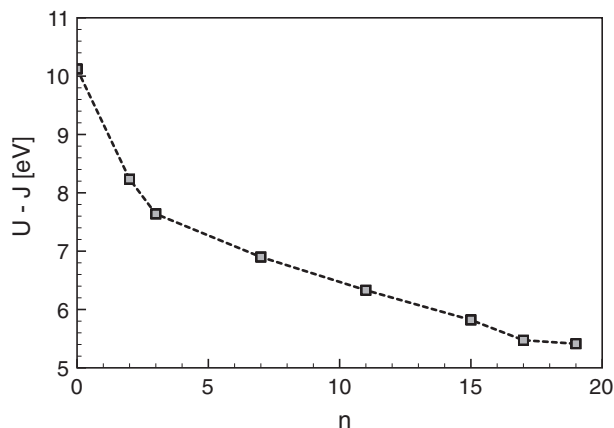

Figure 5. Calculated $U - J$ values for $Pu(OH)_4(H_2O)_n$ for varying n, approaching $U - J = 5.4$ eV for the $n = 19$ cluster. Inclusion of solvent electrostatic effects via a polarizable continuum model (PCM) gives a systematic increase in $U - J$ by about 0.1 eV, for a final value of $U - J = 5.5$ eV at the largest cluster size.

background systematically raises $U - J$ by about 0.1 eV, for a final value of $U - J = 5.5$ eV at $n = 19$. We note that $U - J$ depends mainly on the number of solvating waters, and is relatively insensitive to the details of solvation structure. For example, the CN = 6 and CN = 7 structures from UHF (Table 2) yield a $U - J$ value of 7.77 eV and 7.64 eV, respectively, despite their very different local environments around the Pu(IV) ion. Thus, the $U - J$ derived here is not likely to significantly bias the hydration of $Pu(OH)_4$ towards a specific coordination number. Instead, the on-site terms in the DFT + U act on the Pu 5f-electrons to correct for the destabilization of localized 5f-states (Figure 3, right) and shift them away from the HOMO level.

We further compare DFT + U with wavefunction-based methods for $Pu(OH)_4(H_2O)_3$. Spin–polarized DFT + U calculations are performed using the Vienna *Ab Initio* Simulation Package (VASP) [48], which is a plane-wave implementation of DFT within the projector augmented wave (PAW) formalism. The basis set is truncated at a kinetic energy cutoff of 600 eV. The simulation cell is a 20 Å cube, and only the Γ-point of the Brillouin zone is included. First, we evaluate the energy difference between the CN = 6, 7 structures within the PAW—PBE approximation (no $U - J$ correction). We find that the CN = 6 structure is lower in energy than CN = 7 by 0.14 eV. This is in excellent agreement with the PBE result (0.15 eV) from the Gaussian basis set calculations above, thus supporting the validity of comparing between these two approaches. For $U - J = 7.7$ eV (Figure 5), the DFT + U method finds the CN = 7 structure to be more stable by 0.2 eV, in reasonable agreement with the unrestricted MP2 result of 0.24 eV. Thus, the DFT + U does appear to recover the behavior of the wavefunction-based methods.

While our cluster calculations converge on a seven-coordinate structure for hydrated $Pu(OH)_4$ (Figure 4), we note that drawing conclusions about metal ion coordination numbers in liquid water solely on the basis of the optimized structures of large gas-phase clusters should be done with caution. The optimization methods employed in this work only find local minima and are not guaranteed to deliver a global minimum; robust algorithms for finding the global minimum energy structure on complex energy landscapes remain an open research problem. Our situation is further complicated by the fact that the first coordination shell around Pu(IV) consists of two distinct species, OH^- and H_2O, which leads to a large number of possible structures to consider. Artifacts due to cluster edge effects cannot be completely ruled out despite the presence of two filled solvation shells in the $n = 19$ cluster.

While the aqueous solvation structure of $Pu(OH)_4$ at neutral pH is not known experimentally, various studies employing X-ray absorption techniques have been carried out for the Pu(III) and Pu(IV) aquo ions at low pH, i.e., where the first solvation shell consists entirely of undissociated water molecules. Coordination numbers in the range of 8–10 have been reported [14–16,49], although the experimental determination of coordination numbers can be subject to large errors ranging from 10% to 25% [50]. Our finding of a seven-coordinate structure is at the low end of the experimentally-observed range for the aquo ion at low pH. However, the aquo ion cannot be directly compared to $Pu(OH)_4$ at neutral pH, as the additional Coulomb repulsions between the negatively charged OH^- in $Pu(OH)_4$ is expected to lead to a more open hydration structure. Given the uncertainties in both the experimental and cluster model approaches, in future work, we seek an alternative confirmation for the aqueous hydration structure around $Pu(OH)_4$ via *ab initio* molecular dynamics simulations with periodic boundary conditions, using the parameterization of the DFT + U model as determined in this work.

4. Summary and conclusions

We have carried out a comparison of *ab initio* electronic structure methods for the benchmark case of $Pu(OH)_4$, as a simple model for aqueous Pu(IV) under environmentally relevant concentrations ($< 10^{-12}$ M) and neutral pH. Multi-reference effects involving near-degenerate f-electron configurations do not appear to be significant for the ground state properties examined here, and thus a single-reference theory should, in principle, be adequate. However, single-reference approaches based on DFT with standard approximations for exchange–correlation (PBE and PBE0) prove to be problematic for $Pu(OH)_4$ and small $Pu(OH)_4(H_2O)_n$ clusters, yielding in some cases qualitatively different predictions compared to unrestricted MP2. Thus, for the simulation of $Pu(OH)_4$ in the aqueous phase, we propose the use of DFT + U in order to improve the description of on-site f-electron correlations. We have derived an *ab initio* estimate for the $U - J$ parameter that enters into the DFT + U approach, using small $Pu(OH)_4(H_2O)_n$ ($n = 1 - 19$) clusters to model the dominant effect of nearby water molecules. We

recommend a value of $U - J \sim 5.5$ eV for Pu(OH)$_4$ in liquid water, and thus establish a practical strategy for large-scale dynamical simulations of Pu(IV) chemistry.

Acknowledgments

References

[1] Basic Research Needs for Geosciences: Facilitating 21st Century Energy Systems, US Department of Energy, Office of Basic Energy Sciences, 2007.
[2] Z. Szabó, T. Toraishi, V. Vallet, I. Grenthe, Coord. Chem. Rev. 250 (2006) 784.
[3] G.R. Choppin, J. Radioanal. Nucl. Chem. 273 (2007) 695.
[4] W.R. Penrose, W.L. Polzer, E.H. Essington, D.M. Nelson, K.A. Orlandini, Environ. Sci. Technol. 24 (1990) 228.
[5] A.B. Kersting, D.W. Efurd, D.L. Finnegan, D.J. Rokop, D.K. Smith, J.L. Thompson, Nature 397 (1999) 56.
[6] A.P. Novikov, S.N. Kalmykov, S. Utsunomiya, R.C. Ewing, F. Horreard, A. Merkulov, S.B. Clark, V.V. Tkachev, B.F. Myasoedov, Science 314 (2006) 638.
[7] G.R. Choppin, Mar. Chem. 99 (2006) 83.
[8] V. Neck, J.I. Kim, Radiochim. Acta 89 (2001) 1.
[9] N. Kaltsoyannis, Chem. Soc. Rev. 32 (2003) 9.
[10] V. Vallet, P. Macak, U. Wahlgren, I. Grenthe, Theor. Chem. Acc. 115 (2006) 145.
[11] R.G. Denning, J. Phys. Chem. A 111 (2007) 4125.
[12] S.E. Horowitz, J.B. Marston, J. Chem. Phys. 134 (2011) 064510.
[13] S.O. Odoh, G. Schreckenbach, J. Phys. Chem. A 115 (2011) 14110.
[14] S.D. Conradson, I. Al Mahamid, D.L. Clark, N.J. Hess, E.A. Hudson, M.P. Neu, P.D. Palmer, W.H. Runde, C.D. Tait, Polyhedron 17 (1998) 599.
[15] A.L. Ankudinov, S.D. Conradson, J.M. de Leon, J.J. Rehr, Phys. Rev. B 57 (1998) 7518.
[16] S.D. Conradson, K.D. Abney, B.D. Begg, E.D. Brady, D.L. Clark, C. den Auwer, M. Ding, P.K. Dorhout, F.J. Espinosa-Faller, P.L. Gordon, et al., Inorg. Chem. 43 (2004) 116.
[17] J.A. White, E. Schwegler, G. Galli, F. Gygi, J. Chem. Phys. 113 (2000) 4668.
[18] F.C. Lightstone, E. Schwegler, R.Q. Hood, F. Gygi, G. Galli, Chem. Phys. Lett. 343 (2001) 549.
[19] F.C. Lightstone, E. Schwegler, M. Allesch, F. Gygi, G. Galli, ChemPhysChem 6 (2005) 1745.
[20] P. Nichols, E.J. Bylaska, G.K. Schenter, W. de Jong, J. Chem. Phys. 128 (2008) 124507.
[21] I. Duchemin, F. Gygi, Comput. Phys. Commun. 181 (2010) 855.
[22] M. Guidon, J. Hutter, J. VandeVondele, J. Chem. Theory Comput. 6 (2010) 2348.
[23] E.J. Bylaska, K. Tsemekhman, S.B. Baden, J.H. Weare, H. Jonsson, J. Comput. Chem. 32 (2011) 54.
[24] V.I. Anisimov, F. Aryasetiawan, A.I. Lichtenstein, J. Phys.: Condens. Matter 9 (1997) 767.
[25] P.J. Hay, R.L. Martin, J. Chem. Phys. 109 (1998) 3875.
[26] W. Küchle, M. Dolg, H. Stoll, H. Preuss, J. Chem. Phys. 100 (1994) 7535.
[27] X.Y. Cao, M. Dolg, H. Stoll, J. Chem. Phys. 118 (2003) 487.
[28] T.H. Dunning, J. Chem. Phys. 90 (1989) 1007.
[29] M.W. Schmidt, K.K. Baldridge, J.A. Boatz, S.T. Elbert, M.S. Gordon, J.J. Jensen, S. Koseki, N. Matsunaga, K.A. Nguyen, S. Su, et al., J. Comput. Chem. 14 (1993) 1347.
[30] M.J. Frisch et al., Gaussian 03, Revision D.01, Gaussian, Inc., Wallingford, CT, 2004.
[31] B.O. Roos, Lecture Notes in Quantum Chemistry, in: B.O. Roos (Ed.), vol. 58 of Lecture Notes in Chemistry, Springer-Verlag, Berlin, 1992, p. 177.
[32] M.W. Schmidt, M.S. Gordon, Annu. Rev. Phys. Chem. 49 (1998) 233.
[33] K. Hirao, Chem. Phys. Lett. 190 (1992) 374.
[34] J.P. Perdew, K. Burke, M. Ernzerhof, Phys. Rev. Lett. 77 (1996) 3865.
[35] J.P. Perdew, M. Ernzerhof, K. Burke, J. Chem. Phys. 105 (1996) 9982.
[36] C. Clavaguéra-Sarrio, V. Vallet, D. Maynau, C.J. Marsden, J. Chem. Phys. 121 (2004) 5312.
[37] G. La Macchia, I. Infante, J. Raab, J.K. Gibson, L. Gagliardi, Phys. Chem. Chem. Phys. 10 (2008) 7278.
[38] S. Kümmel, L. Kronik, Rev. Mod. Phys. 80 (2008) 3.
[39] H.J. Kulik, M. Cococcioni, D.A. Scherlis, N. Marzari, Phys. Rev. Lett. 97 (2006) 103001.
[40] A. Sorkin, M.A. Iron, D.G. Truhlar, J. Chem. Theory Comput. 4 (2008) 307.
[41] S.L. Dudarev, G.A. Botton, S.Y. Savrasov, C.J. Humphreys, A.P. Sutton, Phys. Rev. B 57 (1998) 1505.
[42] B. Sun, P. Zhang, X.-G. Zhao, J. Chem. Phys. 128 (2008) 084705.
[43] G. Jomard, B. Amadon, F. Bottin, M. Torrent, Phys. Rev. B 78 (2008) 075125.
[44] M. Cococcioni, S. de Gironcoli, Phys. Rev. B 71 (2005) 035105.
[45] N.J. Mosey, E.A. Carter, Phys. Rev. B 76 (2007) 155123.
[46] N.J. Mosey, P. Liao, E.A. Carter, J. Chem. Phys. 129 (2008) 014103.
[47] S. Miertuš, E. Scrocco, J. Tomasi, Chem. Phys. 55 (1981) 117.
[48] G. Kresse, D. Joubert, Phys. Rev. B 59 (1999) 1758.
[49] P.G. Allen, J.J. Bucher, D.K. Shuh, N.M. Edelstein, T. Reich, Inorg. Chem. 36 (1997) 4676.
[50] J. Chaboy, S. Díaz-Moreno, J. Phys. Chem. A 115 (2011) 2345.